Micro-CT System for Small Animal Imaging

Ki-Yong Nam, Kyong-Woo Kim, Jae Hee Kim, Hyun Hwa Son, Jeong-Hyun Ryu,
Seoung Hoon Kang, Kwon-Su Chon, Seong Hoon Park, Kwon-Ha Yoon

Department of Radiology and Institute for Radiological Imaging Science,
Wonkwang University School of Medicine, Iksan, Korea

We developed a high-resolution micro-CT system based on rotational gantry and flat-panel detector for live mouse imaging. This system is composed primarily of an x-ray source with micro-focal spot size, a CMOS (complementary metal oxide semiconductor) flat panel detector coupled with CsI (Tl) (thallium-doped cesium iodide) scintillator, a linearly moving couch, a rotational gantry coupled with positioning encoder, and a parallel processing system for image data. This system was designed to be of the gantry-rotation type which has several advantages in obtaining CT images of live mice, namely, the relative ease of minimizing the motion artifact of the mice and the capability of administering respiratory anesthesia during scanning. We evaluated the spatial resolution, image contrast, and uniformity of the CT system using CT phantoms. As the results, the spatial resolution of the system was approximately the 11.3 cycles/mm at 10% of the MTF curve, and the radiation dose to the mice was 81.5 mGy. The minimal resolving contrast was found to be less than 46 CT numbers on low-contrast phantom imaging test. We found that the image non-uniformity was approximately 70 CT numbers at a voxel size of $\sim 55 \times 55 \times 100\,\mu m^3$. We present the image test results of the skull and lung, and body of the live mice.

Key Words: Micro-CT, X-rays, In-vivo imaging

INTRODUCTION

In the many research fields such as cancer disease, pathological study, micro-structure morphology, etc., small animals like a mouse have been used commonly. The development of a 3-dimensonal imaging scanner with micro-spatial resolution has been needed because the internal organs or structures of laboratory mice are so small that most of clinical scanners are unable to apply it to the small animals. High-resolution imaging systems required for such small animal studies have allowed researchers to study in-vivo investigation on them, thereby reducing a number of sacrificed animals and allowing the performance of time-progress studies on the same animal specimen. Since a great deal of research and development for the imaging of the small animals was accomplished, many kinds of micro-imaging systems have become developed and nowadays commercially available.[1-5)]

These micro-CT systems have particular characteristics which may result from various factors such as the x-ray source power and its focal spot size, the kind of detectors and its pixel size, geometries to determine the magnification and field of view for the specimens, etc. In some point of view, the micro-CT systems can be categorized by two types, i.e. sample-rotation type and gantry-rotation type. Some early developed CT systems were of the sample rotation type in order to simplify system design and minimize the system control.[6-8)] The sample rotation type, however, could decrease relatively the resolution inherently caused by the motion of a rotating sample as well as the movement of the living sample itself. Moreover, it would be complex to adapt respiratory anesthetic tube into a rotating live animal for the sample-

This work was supported by the Korea Science and Engineering Foundation (KOSEF) grant funded by the Korea government (MOST) (No. M2070403001-07M0403-00110).
Submitted February 16, 2008, Accepted June 12, 2008
Corresponding Author: Kwon-Ha Yoon, Department of Radiology and the Institute for Radiological Imaging Science, Wonkwang University School of Medicine, 344-2, Sinyong-dong, Iksan 570-749, Korea.
Tel: 063)850-6800, Fax: 063)850-6799
E-mail: khy1646@wonkwang.ac.kr

rotation type. For these reasons, we suggest that the gantry-rotation types in micro-CT have some more advantages to enhance spatial resolution and to mitigate various artifacts, but it is true that there have many problems to solve until now. For example, in the case of gantry-rotation type, many techniques, such as precise aligning of every component, weight balancing to minimize the inequivalent angle errors of the rotating gantry, integrated control to synchronize the gantry-angular positioning with a CMOS detector readout time, external trigger timing into the detector, reconstruction techniques and so on, are needed.

We developed a micro-CT system with the rotational gantry-type and the CMOS imaging detector, which could overcome many of the difficult technical problems associated with live mouse imaging. In this study, we present a design, characteristics of the system and 3-dimensional biological imaging results as well as a simulation result of radiation dose on live mouse. As the examples, 2-D reconstruction slices of the body, and 3-D rendered images of the skull of a live mouse using the system are also presented.

MATERIALS AND METHODS

1. Micro-CT System

1) System design and characteristics

The developed in-vivo micro-CT system was designed as a gantry rotation type of x-ray source coupled with an imaging sensor in order to minimize sample movement during scanning. The field of view of the system was determined to be 56 mm×58.6 mm enough to encompass the mouse body. The entire system was composed of a micro focus x-ray source and the CMOS imaging detector, rotational gantry, couch, and parallel imaging data-processing system. The source-to-detector distance is fixed to a distance of 215 mm, and the source-to-object distance is 107 mm. Therefore, the magnification is approximately 2 times.

The spatial resolution of the CT system depends on several factors such as the focal spot size of the x-ray source, the pixel size of the detector, the imaging resolution of phosphor, and sample movement. The focal spot size in an x-ray source, as is well known, gives rise to blurring or a penumbra on the images. The relationship between the blurring and the focal spot size is as follows in (1).

$$U_g=(M-1)\cdot d=2.35\cdot \sigma_b \qquad (1)$$

Where U_g represents the geometric unsharpness, i.e., image blurring, M is magnification, and d is x-ray focal spot size with full-width at half maximum. The lack of sharpness caused by the focal spot size is related to the standard deviation σ_b when the resolution is expressed by the Gaussian model. If the detector array resolution is limited only by the pixel size, the resolution factor σ_d based on the pixel size can be also expressed as the Gaussian function with standard deviation. So, the pixel size factor can be expressed as in (2).

$$\sigma_d \approx M\cdot\frac{1}{2s} \qquad (2)$$

The s in (2) stands for the detector pixel size. When the imaging resolution factor caused by phosphor is expressed as σ_p, and that the contribution of the three main resolution factors, σ_b, σ_d, and σ_p to the total spatial resolution is independent of each other, the propagation law can be applied into the total spatial resolution σ_t of the CT system as in (3).

$$\sigma_t \cong \sqrt{\sigma_b^2+\sigma_d^2+\sigma_p^2} \qquad (3)$$

Using (1), (2), and (3), the total spatial resolution of the designed CT system can be estimated. Referring to the specifications of the x-ray source, the detector, and the phosphor, and inserting these values into the above equations, the expected total resolution of the developed CT system can thus be obtained. We mentioned earlier, in our CT system, the magnification was about 2. Substituting the focal spot size of 5 to 10 μm, the σ_b was obtained within a range of 2.1 to 4.3 μm. The σ_d could also be easily calculated to be 20 μm for a pixel size of 50 μm. Considering the σ_p of the CsI (Tl) phosphor resolution to be in the range of 20 to 40 μm for a phosphor thickness of approximately 200 μm, the expected total spatial resolution of the designed system was estimated to be about 28 to 45 μm according to the phosphor imaging resolutions. We compared the estimated value to the measured value of the developed systems.

2) X-ray source

The anode of the x-ray source we used was a tungsten-targeted material and the window was beryllium with

a thickness of 500 μm (Hamamatsu, Shizuoka, Japan). The maximum power of the source was 39 W in a range of 40 to 130 kVp. The focal spot size could be adjusted by changing the tube currents and voltages. The nominal focal spot sizes of the tube had a range of 5 to 40 μm at a power of 4 to 39 W, respectively. Tungsten was used in collimating the x-ray beam to make cone angle of illumination to approximately 30° for the CT system. An aluminum filter of 200 μm thickness was used to remove low energy x-rays and to reduce any unnecessary radiation dose to the small animals.

3) Image detector

As a recently developed imaging detector, a-Se (amorphous selenium) or a-Si (amorphous silicon) detectors has been used to the imaging system, especially to chest radiography system, or mammography instrument. This kind of detectors is typically categorized to a direct detection method with respect to the CCD, or CMOS, which are belong to the indirect-detection method. The direct detection method has a superior to the indirect one in the special resolution. On the other hand, the frame rate of the direct detection method is relatively inferior. In CT system, total scanning time is important in the view point of radiation damage, especially in the in-vivo experimental testing. Since such the reasons, the a-Si, or a-Se typed-direct detecting sensor have been just applied into some projection diagnostic system. In the future, the figure of merit of the frame rate on the direct detection method will become enhanced enough to apply to the CT system, the better image resolution system could be expected besides of the higher price.

Taking into consideration the larger field of view of the sample, relatively low price and the faster scan speed of the CT system, we selected a CMOS detector (Hamamatsu Photonics K.K, Japan) for the CT system, although it has a relatively higher noise level and larger pixel size than the CCD. It is well known that the field of view is determined by both the effective sensing area of the detector and by the geometric magnification. When the spatial resolution of the system is taken into consideration, the pixel size of the detector is the predominant factor affecting the system resolution. The CMOS detector we used has a pixel size of 50 μm×50 μm, the effective pixel number of 2,240×2,344, and an effective sensing area of approximately 112 mm×117.2 mm, which detector area can be encompassed to the magnified imaging of the mouse size. In our case, the field of view of the sample was ø56 mm, which was sufficient to obtain images in mice of various sizes.

The CMOS detector was coupled with CsI (Tl) scintillator for the conversion of an x-ray to visible light and top-covered by a carbon fiber window of 1 mm thickness. The scintillator thickness in our mode was approximately 200 μm, which was optimized to the hard x-ray energy range for of 20 to 120 keV. The detector output was digitized with a 12 bit dynamic range, and the readout time was 470 ms for single binning and 117 ms for a 4 by 4-binning mode, respectively. Each image signal per one angular degree was read out by an external trigger signal synchronized by an angular-positioning encoder. The angular degree was programmed to be a function of the acquisition view number.

4) Rotational gantry

The gantry was machined to be of 400 mm diameter and 24 mm thickness. It rotates continuously by the step motor with a decrement gear of 100:1. The gantry angular resolution was approximately 0.0072°. The motor was controlled by the motor driver and controller that were interfaced to the computer via RS232 communication ports. The flatness of the gantry measured approximately 4 μm. This value is not serious since it is less than assembling tolerance. The couch was made of acrylic fabric. It is also able to be moved forward and backward by the step motor and had a traveling range of 150 mm. The structure analysis of the designed rotation gantry was simulated using I-DEAS 11 (iCAD, New Delhi, India).

Al6061-T6 (Classified by MatWeb, VA, USA), one of the aluminum alloys, was used in most of the body material of CT system because of its relatively high strength.[9] Applying the weights of the x-ray source (10 kg) and the CMOS detector (3.4 kg) into the modeling, the simulation achieved allowed a maximum and minimum stress of approximately 2.04×10^{2}, and 5.6×10^{-2} mN/mm^2, respectively. As a result, the maximum displacement of the x-ray source and detector was very small with respect to the rotation center, i.e. 500 nm. Fig. 1 shows the system layout of the gantry rotational-type CT system.

5) Alignment of the micro-CT system

The precise alignment was very significant in obtaining images

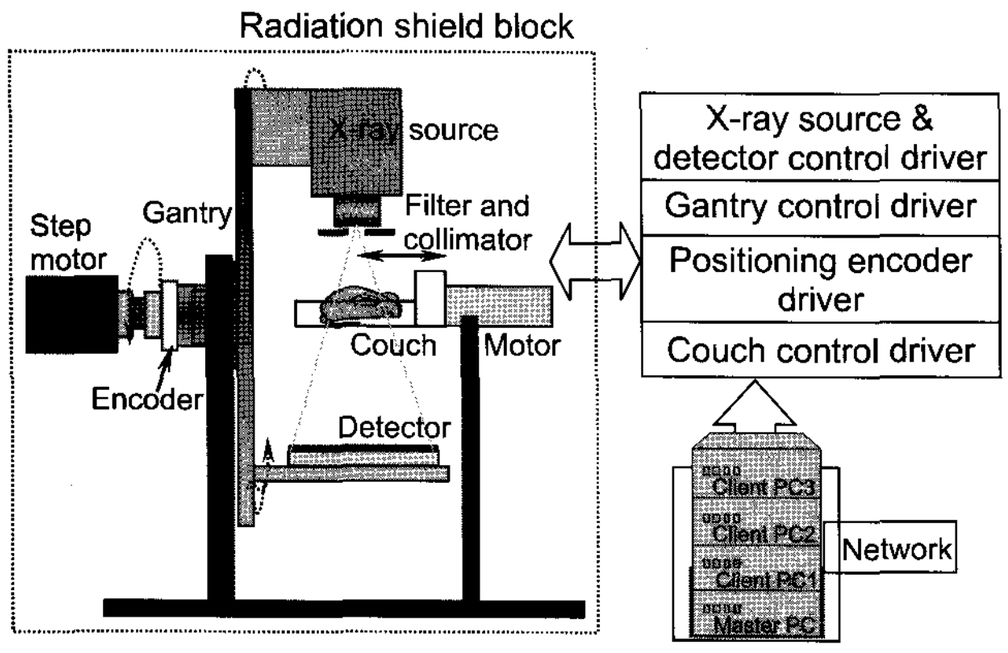

Fig. 1. Layout of the in vivo micro-CT system we developed.

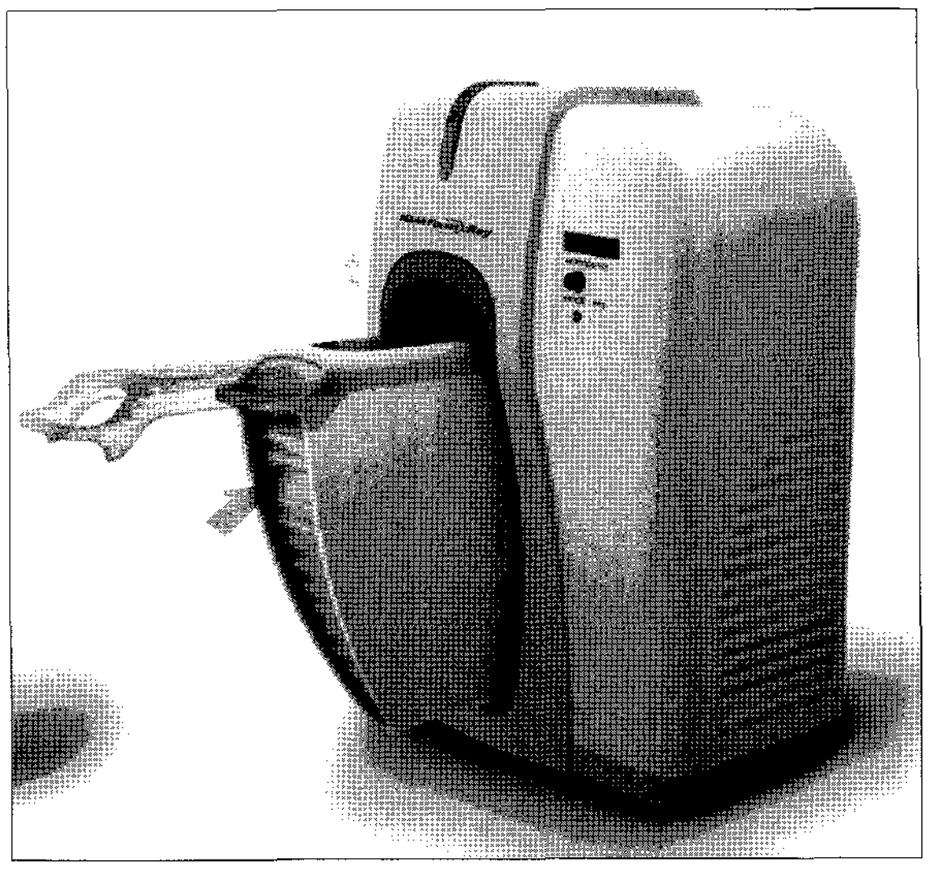

Fig. 2. Photographs of the developed gantry rotational micro-CT system. Note respiratory anesthesia tube for a live mouse on the couch (arrows).

of high-quality spatial resolution with the system. In order to align the detector position with the rotational centered-axis of the gantry and with the x-ray beam center, an alignment phantom was manufactured as referred to a previous manuscript.[6] The phantom was made from a 6 mm thickness of aluminum, and the 17 holes of which has a 1-mm in diameter, were machined to obtain a rectangular configuration. To adjust the position of the holes with respect to the rotational axis and to the beam center, a micrometer was attached to the phantom. With the micrometer, the alignment using the phantom was performed in a manner to match the image of the center hole on the phantom to the detector center, and then to analyze the image shape symmetry of the surrounding holes.

The weight difference between the x-ray tube and the detector was approximately 7 kg. For weight balancing, we measured the angle deviation each time the gantry rotated one degree while keeping the weight unbalanced. While the heavy weight part moves down, the gravity is added to the weight, which gives rise to the relatively larger angle interval of 1 degree. On the other hand, when the weigh part moves up against the gravity, the angle interval become to relatively narrow. In such the way, the value of the angle deviation for one cycle rotation exhibits a sinusoidal. Therefore, the weight unbalance was corrected so as to minimize the amplitude of the sinusoid, with dummy weight adding to the detector side. After balancing weight, we have never found asymmetry problem while the gantry rotates and confirmed no problem in the allowable error range of the angle interval of the gantry motor.

It was important factor for the gantry rotation movement to acquire an image at exactly the defined angle position. In our system, it was set up that a readout timing of an image signal from the detector was synchronized with external trigger signals generated by a positioning encoder of the gantry. The encoder axis coincided with the gantry axis. Fig. 2 shows the photography of the aligned in-vivo micro-CT system.

6) Parallel processing system for reconstruction

Our imaging acquisition system is consisted of an image grabber (National Instruments, TX, USA), and four Pentium IV-based computers using Windows XP OS (Microsoft, USA). The PC system was composed of one host computer and three client computers. The host computer operated as the integrated controller system to move the gantry and couch as well as the detector control including the x-ray source operation. Each data view was saved on the memory of the host computer and simultaneously backed up to the three client computers.

During scanning, each computer performed pre-processing, such as dead pixel corrections, flat-field correction and projection data filtering. The host computer shared the imaging reconstruction process with the client computers. The total reconstruction time for the image size of 1,024×1,024 and for the 512 slices required approximately 2.3 s/slice. Each

computer also becomes performed the back-projection of each one-third of the entire reconstruction. After the back-projections were completed, the partly reconstructed images were combined to make the 2-D final slice images in the host computer. In the reconstruction process, we used commercial software (Exxim Computing, CA, USA) based on the use of a filtered back-projection cone-beam algorithm with A Ram-Lak filter, a band-limiting filter derived from a ramp function.[10] Therefore, each acquired projection image has to be filtered line by line. This was done in the Fourier domain. The filter coefficients to be applied reside in a filter file, which contains the coefficient array represented as 4 byte floats. The filter file representing pure derivates, i.e., Ramp, is 0.0, 1.0, 2.0, 3.0, etc., which corresponds approximately 1,000. Since the filtering is performed as a floating point operation, so the filter coefficients can be scaled. The length of the filter should match the horizontal size of the projection. In our reconstruction process, the horizontal projection size was 1,024 pixels, which corresponds to the filter length of 1,024 elements. The ramp filter was used as a high pass filter. The filers contain N frequency domain coefficients. The cutoff frequency is zero. The input projection was post-processed by smoothing, which is performed by, so-called, slight vertical smoothing mask. In the reconstruction software, one can select one of the several filtering modes with variable range.

7) Small animal imaging protocol

Ten adult male Balb/c mice (Central lab. Animal Inc., Seoul, Korea), ages of 7~11 weeks, were used for this study. The mice were weighed from 22 to 25 g. The mice were placed in an induction chamber with 4% isoflurane in oxygen to induce anesthesia. During imaging, the mice remained anesthetized using 1.5% isoflurane in oxygen; they were allowed to recover between image acquisitions. The mice were injected into the distal tail vein with administration of an iodinated lipid emulsion blood pool contrast agent (Fenestra VC, ART Inc., Canada) at a dose of 0.01 mL/g body weight. Images were obtained at the base line and 10 minutes and 1 hour after contrast injection. All CT image data were acquired using live, free-breathing, and anesthetized mice. All animal studies were carried out in accordance with the regulations of the institutional review board (IRB) of our University.

RESULTS

1. X-ray photon simulation

For the x-ray photon simulation, we used the measured data of x-ray photons emitted from the x-ray source with a tungsten target which was provided by a manufacturer (Hamamatsu, Shizuoka, Japan). The measurement of the x-ray source intensity was performed using a well-calibrated dosemeter (Eberline, FH-40F4, Germany) which was corrected by the accredited calibration machinery. In this case, the x-ray tube was setup to 50 kVp voltage and 65 μA current. This tube set-up condition in our system was determined to be in the way that the mean gray value in a projection image becomes in the mid-range on 16 bit-gray values. We have pursued to comply with the standard guide for computed tomography imaging of ASNT (American Society for Testing and Materials) Designation: E1441-95 as possible. To obtain the initial x-ray intensity in terms of flux, Φ_{flux}, at the position of Be-window, the dose rate to flux conversion equation was used as in (4).[11] In (4), the constant of 0.00873 is induced from air kerma, X is a measured dose rate by the dosemeter, the $(\mu_{en}/\rho)_{air}$ is a x-ray mass energy absorption coefficient of air which is quoted by the NIST (National Institute of Standard and Technology) data, and D (E_i) is a normalized distribution density of an energy, E_i (keV) in the measured x-ray spectrum.[12]

$$\Phi_{flux} = \sum_i \frac{0.00873[R^{-1}] \cdot 6.25 \times 10^{12}[KeV/g]}{E_i(keV) \cdot (\frac{\mu_{en}}{\rho})_{air}} \cdot D(E_i) \cdot X[R/s] \quad (4)$$

The spectrum of the x-ray source was measured using a Si-pin diode detector (XR-100CR, Amptek, USA). All the detectors were displaced about at 0.75 m apart from the x-ray source window. Prior to measure x-ray spectrum, the calibration of the Si-pin diode detector was performed using several well known energy and activities, i.e., ^{55}Fe ($K_{\alpha 1}$ 5.9 keV), ^{109}Cd ($K_{\alpha 1}$ 22 keV) and ^{137}Cs ($K_{\alpha 1}$ 32 keV). To obtain D (E_i), we have normalized the measured number of photon corresponding to each x-ray energy divided by the measured total spectrum. The measured dose rate was then reduced to the value at the Be window position, that is, 155 R/min (@50 kVp, 65 μA). From using for the equation 4, the initial photon

flux was obtained to be $1.26\times10^{10}/cm^2s$, of which was applied to the MCNP simulation program (MCNPx; Los Alamos Lab, TN, USA). In the simulation, the source-to-object distance (SOD) and the source-to-detector distance (SDD) were 107 mm, and 215 mm, respectively. The exposed area and transmission thickness on a mouse were modelled at 40 mm and 40 mm in diameter, respectively. The components of the mice were regarded as the muscle skeleton quoted from the ICRP data (XCOM, NIST, USA).[13] The absorbed dose rate per view was estimated to be 0.19 mGy/s. As the result, the total dose for the scan time of 7 minutes of 360 views was found to be 81.5 mGy.

In the view of point of image quality, the given geometry of SDD and the number of photons arrived on a detector pixel, were related to the signal-to-noise ratio (SNR). We performed the simulation for the total number of photons at detector pixels and obtained the result of 7.84×10^6 photons/cm^2·s. Taking the pixel size of 50 μm×50 μm, the number of photons per pixel was estimated at approximately 2, which is corresponded to the SNR, approximately 1.4.

2. Spatial resolution

The spatial resolution of the CT system was evaluated from the image of the line pattern which had a range 5 to 20 cycles/mm. The x-ray source for the mice was optimized at the conditions of 50 kVp and 65 μA. The line pair pattern was mounted on the center of the couch and exposed to the same x-ray conditions as the mice. By the use of reconstructed CT images of the line pattern, the modulation transfer function (MTF) was obtained as a function of the spatial frequency. The field of view of our CT system as previously mentioned, i.e., 56 mm×58.6 mm (ø45 mm), was designed enough to scan wholly the line pair phantom of size of 30×10 mm^2. So, we mounted the line pair phantom on the couch in the manner that the direction of a series of line pair is perpendicular to the gantry rotation axis, and then scanned the line pair phantom. Once the reconstructed image of the phantom is able to obtain, one of the reconstructed slices also can be obtained as a section (or slice) image of line pair. The section image is resulted in having point-shaped pair image as in Fig. 3 (c). From the projection image of a series of line pair, the wave profile corresponding to the respective line pair number can be obtained. From the wave profile, MTF value was calculated as a function of line pair number. As the same way that the MTF value from the projection image of the line pair phantom was obtained, the MTF from the point-shaped pair image was also obtained. As the results shown in the Fig. 3 (a), white circles and dash line-fitted show the MTF curve from the reconstructed image data, and dark circles and solid line-fitted represent the curve from the projection image data. Fig. 3 (b) and (c) show projected image and reconstructed slice one, and respective fitting curves. The curves at the range of 1 to 5 cycles/mm are almost same. This was happened because the values in the range of 2 to 5 cycles/mm no exist in the line pair phantom, thereby the corresponding MTF values could not have the relevant data. From the fitting result, we confirmed that the difference between 1 and 5 cycles/min was too small to considerate it into the resolution evaluation. The difference between 1 and 5 cycles/mm was obtained to be less than 0.01. One can expect that the MTF result from the projection image

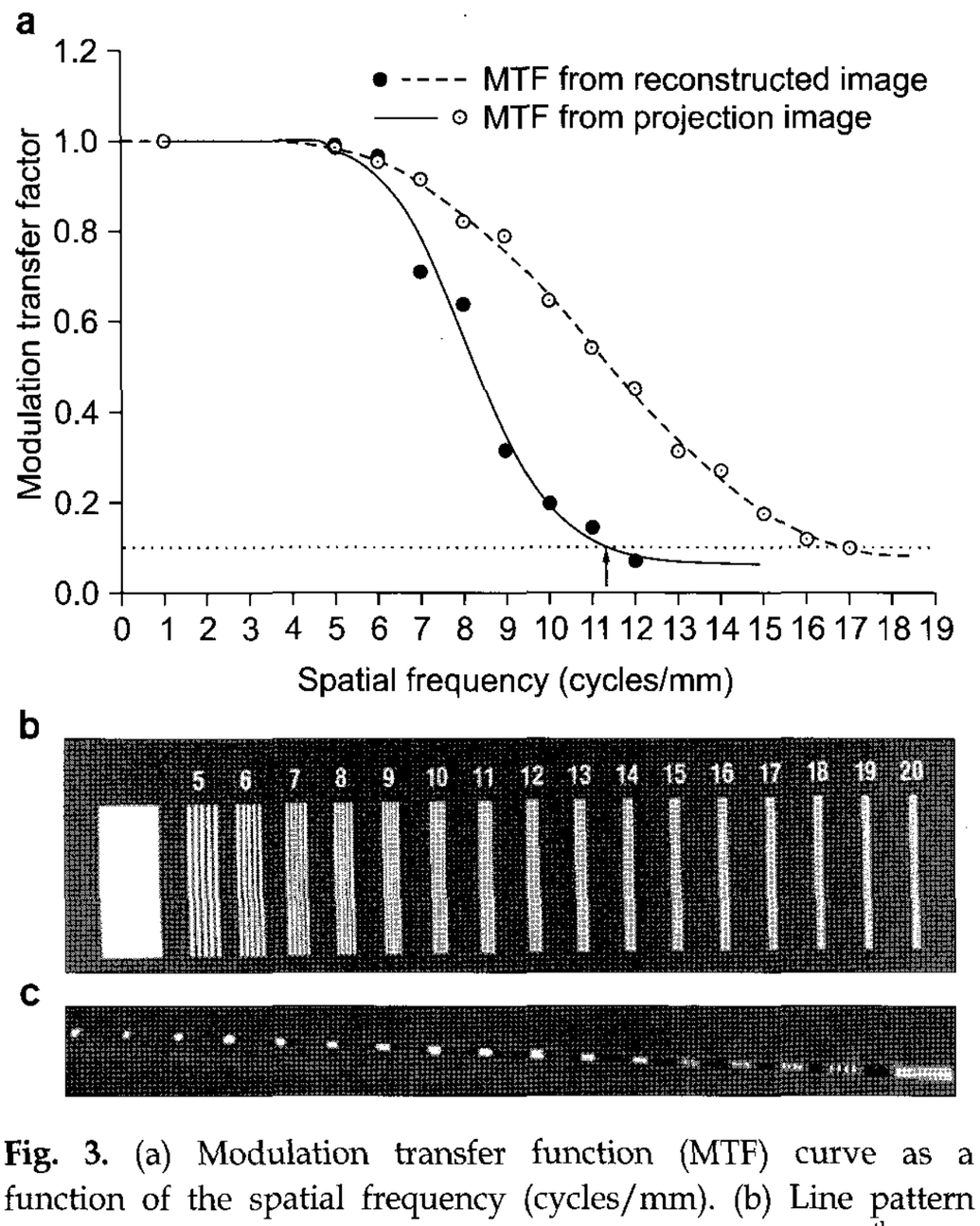

Fig. 3. (a) Modulation transfer function (MTF) curve as a function of the spatial frequency (cycles/mm). (b) Line pattern image applied to the MTF of projection image. (c) 256th slice image of the line pair phantom applied for obtaining the MTF on reconstructed image.

may be superior to that of reconstruction image. In our case, the result of MTF from the projection image was better than the reconstructed one. We suggest for the reason that the blurring was not removed artificially throughout reconstruction process in order to compare both cases inherently. By the hand, pre-processing was done by the smoothing filtering as well as flat field and off-set corrections.

The 10% point on the MTF curve corresponds to 17 cycles/mm for the projection image of the line pattern, while the spatial resolution for the reconstructed image of the identical line pattern corresponds to the 11.3 cycles/mm. It could be considered that the several factors including applicable kind of imaging filters or reconstruction filter, and system alignment condition determined the spatial resolution for the reconstructed image. The measured spatial resolution values had a near range of the expected total spatial resolution of the $28 \sim 45\,\mu$m. From the obtained value of $30\,\mu$m, the resolution σ_p for the CsI (Tl) phosphor of $200\,\mu$m thickness could be induced by using (3), which resulted in approximately $22\,\mu$m.

3. Image analysis using a phantom

The beam quality for an image evaluation is important. There are some beam quality indicators as an international standard testing and material, such as ASNT (American Society for Testing and Materials). In our study, we did not use such tool or standards. But, we have used CT phantom of QRM GmBH, which is another kind of phantom and frequently used to evaluate CT imaging. We also complied with the designation E 1441-95 of ASNT. Screening condition was determined as in the way that the radiation dose of the animal sample becomes minimized and the mean gray value of a projection view is distributed in the mid-range in the gray value of 16 bit dynamic range.

We evaluated contrast noise and uniformity using a contrast phantom (QRM-MicroCT-HA, Germany). The phantom contained symmetrically arranged cylindrical inserts with five kinds of densities of HA (calcium hydroxyapatite), as shown in Table 1. The attached number of HA in the phantom means the corresponding CT numbers of the HA phantoms. The diameter and length of the phantom were 32 mm and 38 mm, respectively. The diameter and length of the inserts were 5 mm and 38 mm respectively. The phantom body was constructed of epoxy resin which is equivalent to the CT number of water. Prior to the CT image analysis, the CT calibration was performed by using the water and air. After the CT calibration, we have applied the QRM phantom.

Fig. 4 shows the phantom scheme and the reconstructed phantom image with a voxel size of $\sim 100\times100\times100\,\mu m^3$. According to the definition of contrast-to-noise ratio (CNR) as expressed in (4), we obtained the CNR from the measured mean CT number and calculated the standard deviation of a given ROI on the insert image at the 50 kVp.

$$CNR = \frac{CT\#}{\sigma} \tag{4}$$

In (4), the CT # and σ denote the CT number and standard deviation of pixel values on a given region of interest, respectively. The measured mean CT numbers and CNR of the

Table 1. Measured mean CT numbers and the CNRs of the inserts in the phantom.

Inserts	mgHA/cm^3 (HU)	Density (g/cm^3)	Measured mean CT number and (CNR) at 50 kVp
HA50	50	1.16	46 (1.5)
HA200	200	1.26	200 (4.7)
HA800	800	1.66	789 (8.7)
HA1200	1,200	1.86	1,120 (7.2)

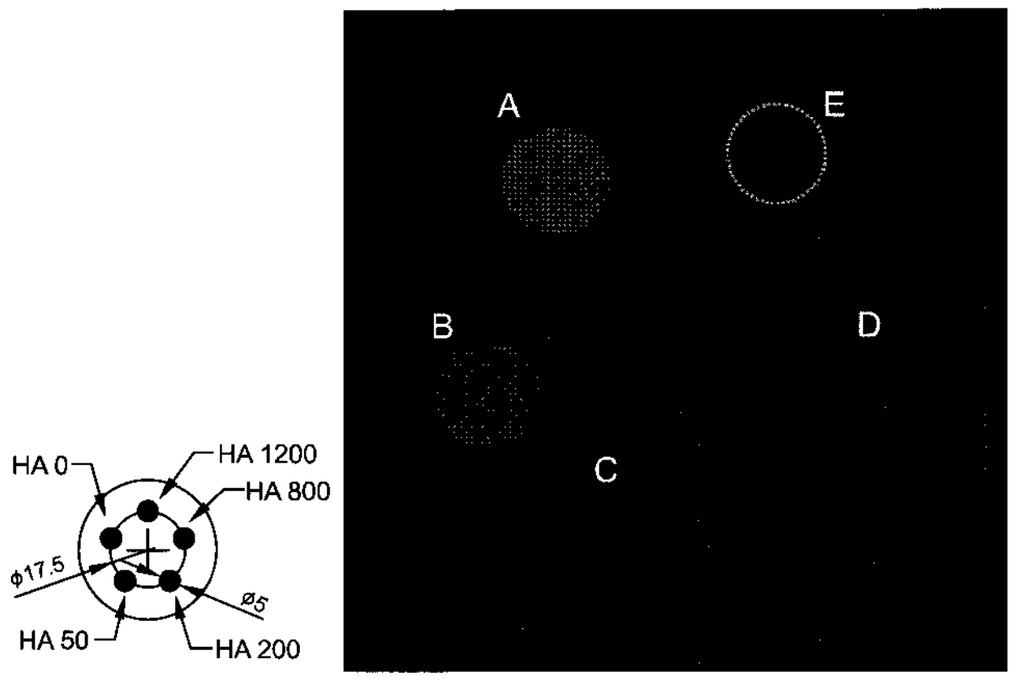

Fig. 4. The phantom scheme (left) and the reconstructed phantom image (right) with a voxel size of $50\times50\times100\,\mu m^3$. A, B, C, D, and E corresponds to HA 1200, HA 800, HA 200, HA 50, and HA 0, respectively.

inserts are also given in Table 1. The phantom image shown in Fig. 4 and Fig. 5 was reconstructed in an image size of 1,024×1,024×512 and then image-processed by the median filter in order to reduce ring artifact. However, this demonstrated that the ring artifact could not be completely eliminated. We assumed that the ring artifact in the reconstructed image was caused by the non-uniform sensitivity of the detector pixels with time-variance, although we performed imaging processing with both the flat-field correction and dead pixel correction of the detector. Such conjecture was based on the fact that the quantum efficiency (DQE) of the pixel in most detectors was not stable, but varied with time variance, which means that each pixel value has a different value according to every frame number.[14] In the CT system we developed, the minimal resolving contrast was estimated to be 46 CT numbers as in Fig. 4 and Table 1. In the CT phantom image shown in Fig. 4, the material of HA0 insert is equal to that of the phantom body, so that they have identical CT number.

For the uniformity evaluation of the reconstruction image, we used a water phantom made of water-equivalent plastic with an outer-diameter of 30 mm. Fig. 5 shows how the CT calibration was well done as well as the uniformity of the reconstructed transaxial image signals, which was obtained from two axial profiles, i.e., a- and b-directions. From Fig. 5, the standard deviation of the CT signals on the water region was resulted in 70 CT numbers. We can aware of the CT numbers roughly for the air, water and plastic in the Fig 5. The measured mean CT numbers for the inserts was remarked in Table 1.

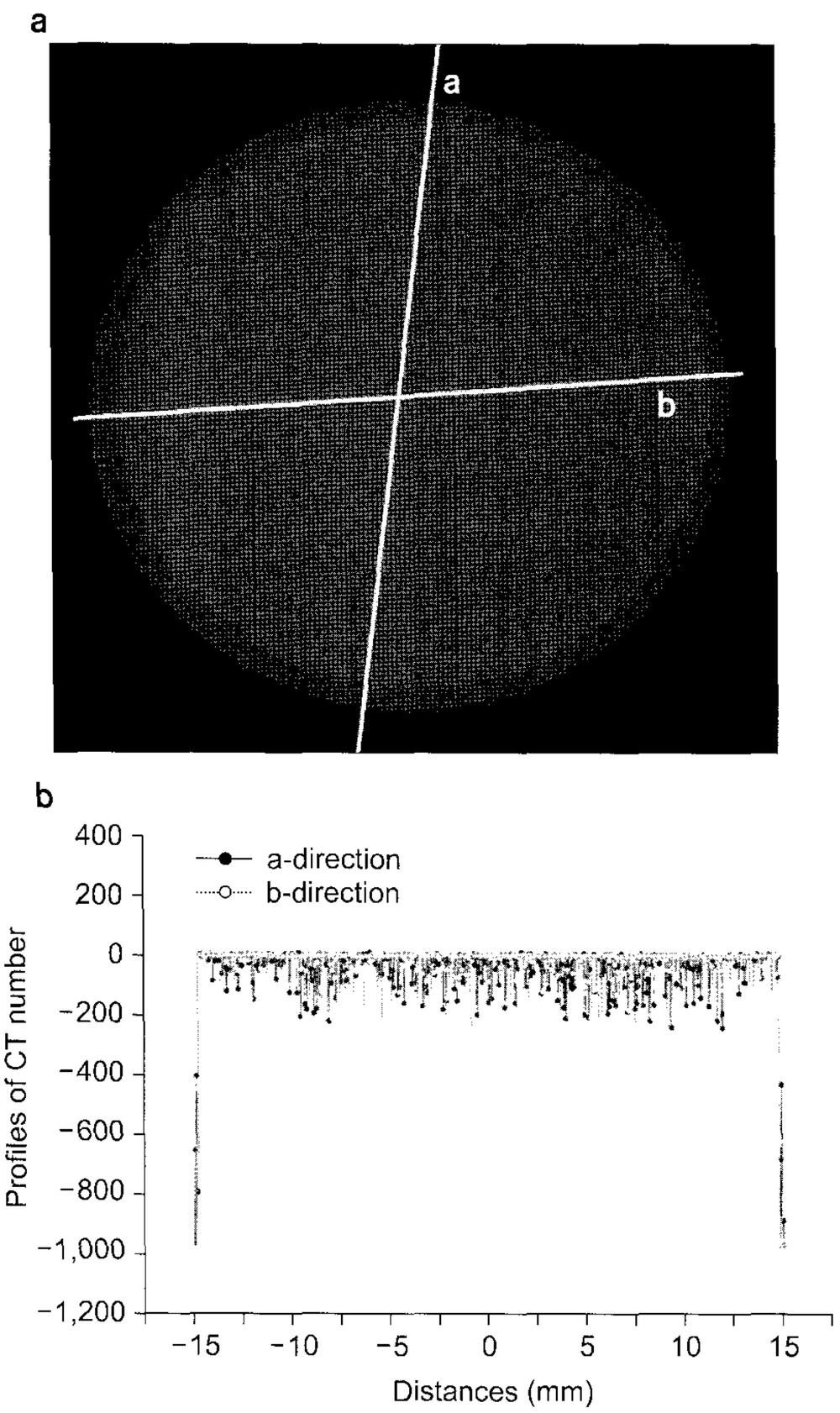

Fig. 5. Uniformity profile of the reconstructed water phantom. (a) Transaxial image of the water phantom, and (b) the CT number profile of the transaxial image in a radial direction. The standard deviation of the signal profile is 20 CT numbers.

4. In-vivo CT images

We obtained reconstructed images on live mice using our developed micro-CT system. The characteristics of the micro-CT system we d eveloped are summarized in Table 2. Our raw data was acquired under the same experimental conditions. The number of views of 360 was applied to the reconstruction process. It took for a projection to image a total of 1.16 seconds per view, i.e. 0.74 second for the exposure time, and 0.42 second for the readout time including a gantry rotation time. The total scanning time eventually took approximately 7 minutes (1.16 s×360 views). As the scan time was mainly dependant of the detector readout speed or frame rate, the minimum scan time for 360 views in this system could be shortened to approximately 1.7 minutes for the 4 by 4 pixel binning mode.

As the reconstruction image size was 1,024×1,024 pixels and 512 slices, and the time to reconstruction per slice took about 2.3 seconds, the total reconstruction time required to obtain the 512 slices was approximately to be 20 minutes. The entire reconstructed data was converted to the DICOM (Digital Imaging and Communications in Medicine) format, and transformed to 3D-rendered imaging by using 3D rendering

software, Lucion (MeviSYS, Seoul, South Korea).

Fig. 6 shows the skull and cerebral vessels of a live mouse with respiratory anesthesia. Fig. 7 shows sagittal and coronal reconstructed images of the mouse body after administration of an iodinated lipid emulsion blood pool contrast agent. Although respiratory triggering was not performed, these images very clearly show the vascular structure of the inferior vena cava and porto-mesenteric venous system without motion artifacts.

DISCUSSION

We developed a micro-CT system including an x-ray source and a flat panel detector coupled with rotation gantry for live mice studies. As demonstrated in Fig. 6 and Fig. 7, the ability to visualize the heart and lung may provide pathologically and anatomically important information for biomedical research. For in vivo studies of live mice, the scan time must be as short as possible.

To obtain a micro-CT image, the elements must be aligned very accurately in the designated position as position errors because the deterioration in the image quality and at worst makes the image invisible. Because the CT images are

Table 2. Characteristics of the micro CT system. The value of mgHA/cm^3 is equivalent to the HU unit.

Contents	Characteristics
Spatial resolution (MTF)	11.3 cycles/mm
X-ray tube voltage	40~130 kVp
Field of view	56 mm×59 mm (ø 45 mm)
Magnification	2×
Dimensions	1200 (W) mm×1255 (H) mm×1500 mm
Source to detector distance	215 mm
Source to object distance	107 mm
Cone beam angle	30°
Scan time for one view	1.15 s
Reconstruction time per slice	2.3 s/slice
Reconstruction algorithm	Filtered feldkamp back projection

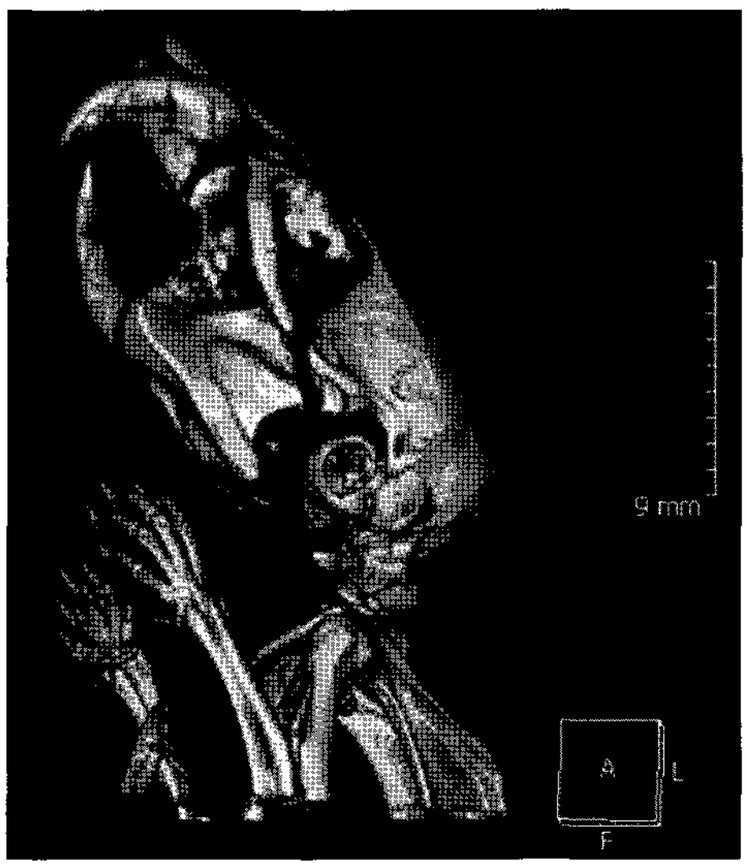

Fig. 6. 3D image of the skull and cerebral vessels of a live mouse after administration of a blood-pool contrast agent.

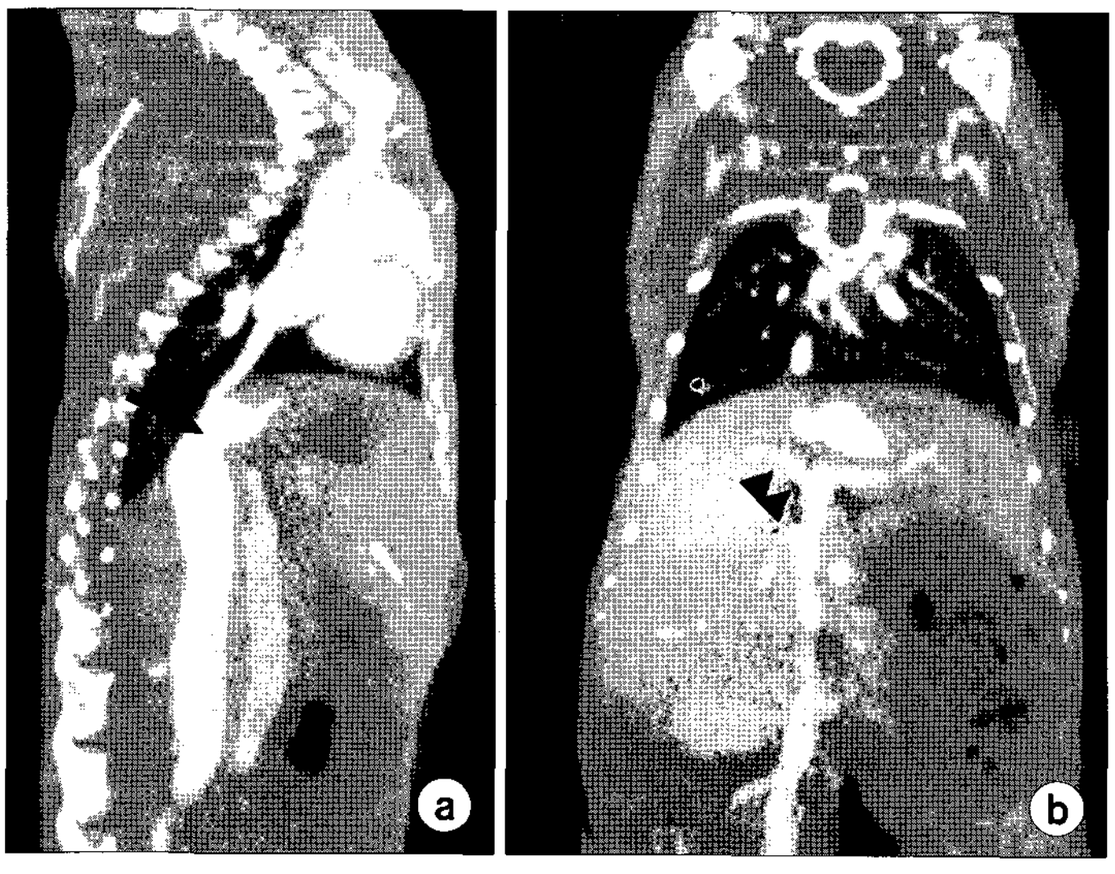

Fig. 7. Sagittal (a) and coronal (b) reformated images of a live mouse body after administration of a blood-pool contrast agent. The inferior vena cava (arrow) and porto-mesenteric venous system (arrowheads) are clearly visible.

reconstructed from raw images of 360 degrees and the focal spot size of the x-ray source and pixel size of the detector are small, alignment requires at least minimum micron tolerances. Therefore, the proper method for alignment is required, and all of the elements must be controlled. The alignment of the detector to the x-ray source at the CT body was the most tedious work. We used the special alignment phantom above mentioned.

The radiation dose to the animal is an important concern when developing a micro-CT system. In general, an exposure of 2 Gy is considered a lethal dose after which 50% of all mice die (LD50). In case that threshold of x-ray irradiation affect on the organ and tissue metabolism is unclear, the exposure to the animal must be minimized on scanners that perform multiple sequential scans. For micro-CT, a dose of 0.5 ~1.0 Gy is generally required, and this represents approximately 5% of a lethal dose 50/30 (50% of animals die within 30 days) in mature mice.[5] In our CT system, it was confirmed as a result of simulation that the total dose after scanning with 360 projections was 81.5 mGy, which was in the allowable radiation dose range required to keep an animal alive.

The averages of the heart and breathing rates of a mouse are approximately 250~300 pulse/minute and 50~60 pulse/minute, respectively. The heart and breathing motion predominantly affects the morphological and functional analysis of this small animal using a micro CT system. For example, when a researcher wishes to determine the lung tumor volume in vivo mice in preclinical lung cancer research, the motion artifact from breathing can make it difficult to obtain an accurate assessment. To overcome this problem, cardiac- and respiratory-gated micro CT imaging methods have been introduced.[15,16] We believe that the micro-CT system developed is also adaptable to the cardiac- and respiratory-gating systems for in vivo heart and lung imaging. However, as a disadvantage of the CT system, the scan time of this CT is not yet enough to obtain cardiac image. It is well known that the monochromatic x-ray beam enhances the image quality. To enhance image contrast, some research groups have tried to make it more quasi-monochromatic using many kinds of filters and anode targets.[17,18] In this study, we have not presented the study of various filter tests to make quasimonochromatic x-ray beam condition. We will further study on the optimistic combination of the filter materials to enhance x-ray beam condition.

In addition, advanced scan CT systems with the capability of higher speed scanning using slip ring technology, have recently been introduced.[19] Therefore, further studies must be done in order to improve the spatial and temporal resolution of the micro-CT systems for wider application of small animal imaging. The images shown in Fig 6, 7 have some kinds of artifact. We guess that those artifacts are due to the sensitivity variation of the detector pixels with respect to time. So, we will continue to study on the enhanced image correction method to mitigate the artifact.

In conclusion, we have developed a gantry rotation type micro-CT system for the purpose of live mouse studies. We have been able to investigate the heart and lung as well as the vascular structure of the inferior vena cava and porto-mesenteric venous system by using this micro-CT system. As a result of this study, we would like to suggest that the gantry rotation type CT has several advantages, in particular, minimizing specimen movement, and the ability to configure the cardiac- and respiratory-gated system according to the specimen even though the aligning process is more difficult and tedious than that of sample rotation type of micro-CT. Therefore, we have confirmed that the developed gantry rotational CT system can be used successfully for in vivo mouse imaging studies.

REREFENCES

1. **Paulus MJ, Gleason SS, Kennel SJ, Hunsicker PR, and Johnson DK**: High resolution X-ray computed tomography: an emerging tool for small animal cancer research. Neoplasia 2:62-70 (2000)
2. **Paulus MJ, Gleason SS, Easterly ME, Foltz CJ**: A review of high-resolution X-ray computed tomography and other imaging modalities for small animal research. Lab Anim (NY) 30:36-45 (2001)
3. **Davis GR, Elliott JC**: X-ray micro tomography scanner using time-delay integration for elimination of ring artifacts in the reconstructed image. Nucl. Instrum. Methods in Phys Res A394:157-162 (1997)
4. **Holdsworth D, Drangova M, Fenster A**: A high-resolution XRII-based quantitative volume CT scanner. Med Phys 20: 449-462 (1993)
5. **Ritman EL**: Micro-computed tomography-current status and developments. Annu Rev Biomed Eng 6:185-208 (2004)

6. **Chun IK, Cho MH, Lee SC, Cho MH, Lee SY**: X-ray micro-tomography system for small-animal imaging with zoom-in imaging capability. Phys Med Biol 49:3889-3902 (2004)
7. **Lee SC, Kim HK, Chun IK, Cho MH, Lee SY, Cho MH**: A flat-panel detector based micro-CT system: performance evaluation for small-animal imaging. Phys Med Biol 48:4173-4185 (2003)
8. **Sakellariou A, Senden TJ, Sawkins TJ, et al**: An x-ray tomography facility for quantitative prediction of mechanical and transport properties in geological, biological and synthetic systems. *Proceeding of SPIE 5535.* 2004, Denver, pp.473.
9. **http://www.matweb.com/search/search.asp**
10. **Feldkamp LA, Davis LC and Kress JW**: Practical cone-beam algorithm. J Opt Soc Am A1:612-619 (1984)
11. **Boone JM, Velazquez O, Cherry SR**: Small-animal X-ray Dose from Micro-CT. Molecular Imaging 3:149-158 (2004)
12. **http://physics.nist.gov/PhysRefData/Xcom/html/xcom1.html**
13. **http://physics.nist.gov/PhysRefData/**
14. **Goertzen LA, Nagarkar V, Street RA, Paulus MJ, Boone JM, Cherry SR**: A comparisonof x-ray detectors for mouse CT imaging. Phys Med Biol 49:5251-5265 (2004)
15. **Bader CT, Fubara B, Hedlund LW, Johnson GA**: 4-D micro-CT of the heart. Molecular Imaging, 4:110-116 (2005)
16. **Cody DD, Nelson CL, Bradley WM, et al**: Murine lung tumor measurement using respiratory-gated micro-computed tomography. Invest Radiol 40:263-269 (2005)
17. **Mckinley RL, Tornai MP, Samei E, Bradshaw ML**: Initial *study of quasi-monochromatic X-ray beam performance for* X-ray computed mammotomography. IEEE Trans. Nucl Sci 52:1243-1250 (2005)
18. **Chen B, Ning R**: Cone-beam volume CT mammographic imaging feasibility study. Med Phys 29:755-770 (2002)
19. **Cody DD, Cavanaugh D, Price RE, Rivera B, Gladish GW, Travis E**: Lung imaging of laboratory rodents in vivo. *Proceeding of SPIE* 5535. 2004, Denver, pp43.

소동물영상을 위한 마이크로 컴퓨터단층촬영장치

원광대학교 의과대학 영상의학교실 및 익산방사선영상과학연구소

남기용 · 김경우 · 김재희 · 손현화 · 유종현 · 강성훈 · 천권수 · 박성훈 · 윤권하

살아있는 마우스 영상화를 목적으로 겐트리 회전형과 평판영상검출기를 기반으로 한 고분해능 마이크로 컴퓨터단층촬영장치를 개발하였다. 이 장치는 주로, 마이크로 크기 광원사이즈를 갖는 X-선 광원, CsI (Tl)과 결합된 평판형 상보성 금속산화 반도체 영상검출기(CMOS), 선형이송 카우치, 위치정보 엔코더와 결합된 겐트리, 그리고 영상데이터 처리를 위한 병렬처리 시스템으로 구성되었다. 본 장치는 겐트리 회전형으로 설계되었는데, 이는 살아있는 마우스를 CT 영상을 얻는데 있어서 마우스 움직임에 기인한 영상결점의 최소화에 유리하고 촬영하는 동안 쥐의 호흡마취시행에 여러 가지 장점을 갖기 때문이다. CT 팬텀을 이용하여 개발한 CT 장치의 공간해상도, 영상대비도 그리고 영상균일도를 평가하였다. 결과로써, 본 장치의 공간해상도는 MTF 곡선으로부터 10%에 해당하는 약 11.3 cycles/mm을 얻었으며, 마우스에 대한 방사선 피폭선량은 81.5 mGy의 결과를 얻었다. 저대비 영상팬텀을 이용한 영상실험에서 분해가능 최소영상대비차는 약 46 CT였다. 55×55×100 μm^3의 복셀(voxel) 크기에서 영상의 불균일도는 약 70 CT 임을 얻었다. 또한 본 연구에서는 살아있는 마우스의 몸체, 뼈, 그리고 간에 대한 영상 테스트 결과를 제시하였다.

중심단어: 마이크로 CT, 엑스선, 생체영상